Recent measurements of identified hadron spectra and multiplicities in Be+Be and Ar+Sc collisions at SPS energies

Maciej P. Lewicki[*]

for the NA61/SHINE Collaboration
University of Wrocław
E-mail: malewick@cern.ch

NA61/SHINE is a fixed target experiment at the CERN Super Proton Synchrotron. The main goals of the experiment are to discover the critical point of strongly interacting matter and to study the properties of the onset of deconfinement. In order to reach these goals, a study of hadron production properties is performed in nucleus-nucleus, proton-proton and proton-nucleus interactions as a function of collision energy and size of the colliding nuclei. In this talk, the newest preliminary results on identified hadron spectra produced in Ar+Sc and Be+Be collisions at six beam momenta (13A, 19A, 30A, 40A, 75A and 150A GeV/c) will be shown. The kinematic distributions and measured multiplicities of identified hadrons will be compared with NA61/SHINE and NA49 p+p and Pb+Pb results, as well as with available world data.

Corfu Summer Institute 2018 "School and Workshops on Elementary Particle Physics and Gravity"
(CORFU2018)
31 August - 28 September, 2018
Corfu, Greece

---

[*]Speaker.

1. Introduction

NA61/SHINE is a fixed target spectrometer [1] located in CERN's North Area, utilizing the SPS proton, ion and hadron beams. Tracking capabilities are provided by four large volume Time Projection Chambers (TPC), two of which are located in magnetic fields. The Projectile Spectator Detector (PSD), a zero degree, modular calorimeter, is used to determine the centrality of the collisions.

The aim of the experiment is to explore the QCD phase diagram (μ_B, T) by a two-dimensional scan in collision energy and system size. The yields of hadrons produced in the collisions are studied for indications of the onset of deconfinement [2] and the critical point of the phase transition [3]. This paper discusses the analysis of Ar+Sc and Be+Be collisions, the next step of the system size scan, following the earlier analysis of p+p reactions. Comparison of obtained hadron spectra gives an important insight into the dynamics of ion collisions in the transition region between reactions of light and heavy nuclei.

2. Particle Identification Methods

Charged particle identification in NA61/SHINE is based on the measurement of the ionization energy loss dE/dx in the gas of the TPCs and the time of flight tof obtained from the ToF-L and ToF-R walls. In the region of the relativistic rise of the ionization at large momenta the measurement of dE/dx alone allows particle identification. At lower momenta, namely $|\vec{p}| \leq 7\text{GeV}/c$, the peaks of protons and kaons in dE/dx distributions overlap and the quality of the particle identification is ensured with supplementary measurements of mass (m^2) with time of flight detectors. The combined acceptance region of these identification methods in the analysis of Be+Be collisions can be seen in Fig. 3 for each employed beam momentum.

The contributions of $e^+, e^-, \pi^+, \pi^-, K^+, K^-, p, \bar{p}$ and d are obtained by fitting the dE/dx and m^2-$dEdx$ distributions separately for positively and negatively charged particles in bins of laboratory momentum p_{lab} and transverse momentum p_T (see Ref. [4] for details).

In fits to the dE/dx distributions the signal shape for a given particle type is parametrized as the sum of asymmetric Gaussians with widths $\sigma_{i,l}$ depending on the particle type i and the number of points l measured in the TPCs. Simplifying the notation in the fit formulas, the peak position of the dE/dx distribution for particle type i is denoted as x_i . The contribution of a reconstructed particle track to the fit function reads:

$$f(x) \;=\; \sum_{i=p,K,\pi,e,d} N_i \frac{1}{\sum_l n_l} \sum_l \frac{n_l}{\sqrt{2\pi}\,\sigma_{i,l}} \, \exp\left[-\frac{1}{2}\left(\frac{x-x_i}{(1\pm\delta)\,\sigma_{i,l}}\right)^2\right] \tag{2.1}$$

where x is the dE/dx of the particle, n_l is the number of tracks with number of points l in the sample and N_i is the amplitude of the contribution of particles of type i. The second sum is the weighted average of the line-shapes from the different numbers of measured points (proportional to track-length) in the sample. The quantity $\sigma_{i,l}$ is written as:

$$\sigma_{i,l} = \frac{\sigma_0}{\sqrt{l}} \left(\frac{x_i}{x_\pi}\right)^\alpha \tag{2.2}$$

where σ_0 is assumed to be common for all particle types and $\alpha = 0.625$ is a universal constant (pre-fit to the whole dataset).

In case of fitting m^2-$dEdx$ distributions the formula becomes two-dimensional. The dependence on energy loss dE/dx can be simplified into Gauss function as we expect similar track lengths within a kinematic bin. The m^2 dependence is assumed to be described by a sum of two Gaussians with common mean, but different widths and amplitudes. To keep notation compact x and y denote dE/dx and m^2 measurements respectively:

$$f(x,y) = \sum_{i=p,K,\pi,e,d} N_i \exp\left[-\frac{(x-x_i)^2}{2\sigma_x}\right] \left(f \exp\left[-\frac{(y-y_i)^2}{2\sigma_{y_1}^2}\right] + (1-f) \exp\left[-\frac{(y-y_i)^2}{2\sigma_{y_2}^2}\right] \right) \tag{2.3}$$
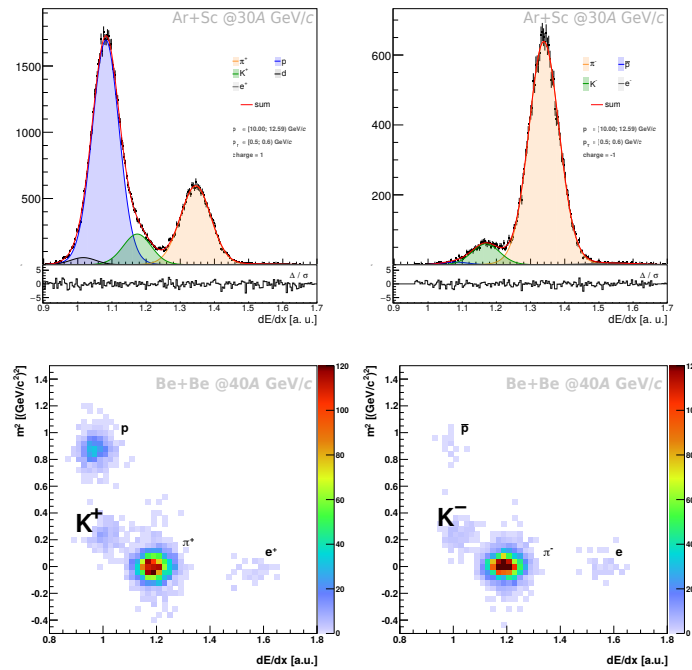

Figure 1: Particle identification methods in NA61/SHINE. The primary method is based on measuring the energy loss per unit length (dE/dx) of a particle traversing the gas in the time projection chambers (top). For particle momenta ≤ 7 GeV/c measurement of dE/dx is not sufficient (the peaks of kaons and protons overlap) and it is supplemented by the measurement of mass derived from time of flight data (vertical axis on bottom plot).

Fits obtained in (p_{lab}, p_T) bins can now be used to calculate the probability of a given particle being one of the studied species $i = \pi^\pm, K^\pm, p, \bar{p}, e^\pm, d$:

$$P_i(p, p_T, {}^{dE/dx}) = \frac{f_i(p, p_T, {}^{dE/dx})}{\sum_i f_i(p, p_T, {}^{dE/dx})} \tag{2.4}$$

The probability P_i is used to populate the histograms in rapidity y and transverse momentum p_T for given charged hadron species. Each measured particle enters the histogram with a weight equal to the probability calculated with Eq. 2.4. Thus the number n_i of particles of type i in a given

bin can be calculated as:

$$n_{i \in \{\pi^\pm, K^\pm, p, \bar{p}, e^\pm, d\}} \quad = \quad \sum_{j=1}^{m} P_i\left(p, p_T, {}^{dE}\!/\!{}_{dx}\right) \tag{2.5}$$

where the summation runs over the number of particles *m* that belong to this bin. This procedure was proposed in Ref. [5] and was called the "identity method" . In this way particle yields can be calculated with very high precision even though the direct track by track identification is not possible.

3. Data analysis

3.1 Event selection

The events recorded by the NA61/SHINE spectrometer were selected for a well reconstructed interaction vertex in the target and the centrality of the collisions. Event centrality classes were determined using the PSD calorimeter, located most downstream on the beam line. It measures predominantly the energy E_F carried by projectile spectators, the non-interacting nucleons of the beam nucleus. The distribution of E_F was used to define and select event classes corresponding to collision centrality intervals (see Fig. 2).
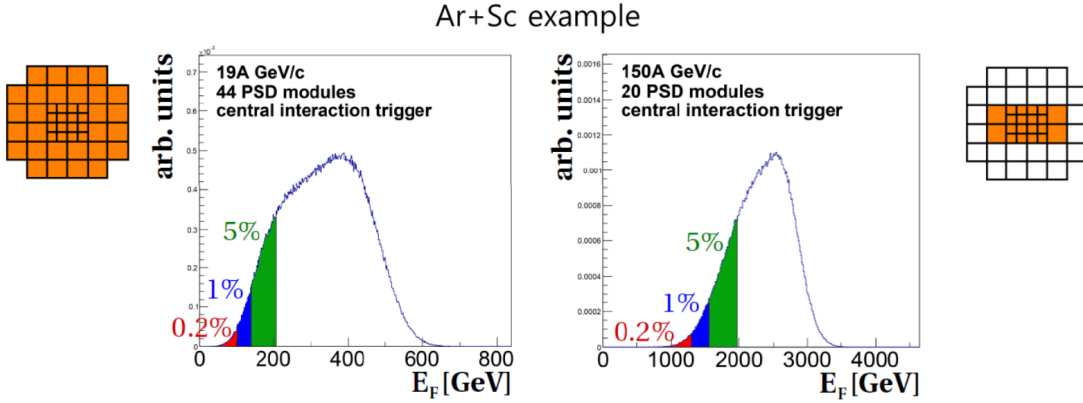

Figure 2: Event centrality selection using the forward energy (E_F) measured by the PSD calorimeter. Distributions of E_F are shown for 19*A* (left) and 150*A* GeV/*c* (right) beam momentum. Orange shaded areas on the front face diagram of the PSD indicate modules selected for calculation of E_F. Choice of modules is based on correlation studies between E_F and track multiplicity measured by the TPCs.

3.2 Corrections and errors

Corrections of the raw data were based on simulations using the EPOS-1.99 [6] (version CRMC 1.5.3.) model and the GEANT-3.2 code for particle transport and detector simulation (see Ref. [7]). Centrality classes in the model calculations were selected by the number of forward spectator nucleons.

Ar+Sc results presented in the plots are shown with statistical uncertainties only. These come from two sources: the experimental data and the simulation-based corrections. The contribution of the latter is insignificant ($< 0.1\%$).

Based on the previous analysis of p+p [4, 7] reactions, systematic errors were estimated at a level of 5%-10%.

4. Identified Hadron Spectra

Using well measured tracks coming from the primary interaction, double differential yields per event in bins of momentum and transverse momentum were obtained using the identification methods described in the previous section. Double differential yields per event $\frac{1}{N}\frac{d^2n}{dy\,dp_T}$ are shown in Fig. 3. Note the large acceptance extending down to $p_T=0$, an important advantage of fixed-target experiments. Figure 4 shows transverse mass spectra of kaons (K^+, K^-) at mid-rapidity. Similarly as for other colliding systems (p+p and Pb+Pb) kaon m_T spectra do not show significant deviations from the exponential function fitted to the data points.
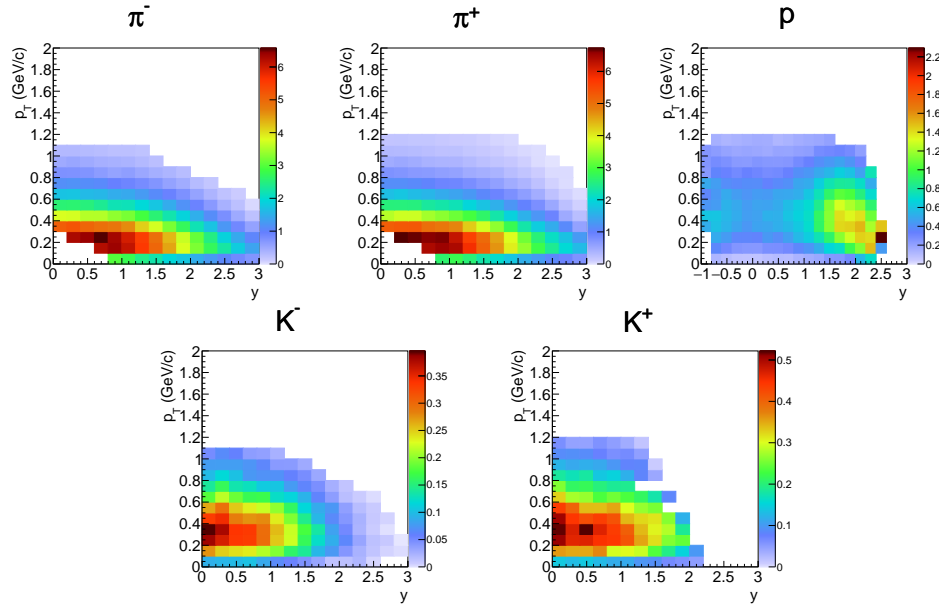

Figure 3: Spectra in rapidity y and transverse momentum p_T of identified charged hadrons produced in the 20% most central Be+Be collisions at 150A GeV/c – preliminary results.

In order to obtain dn/dy yields, the data is extrapolated in p_T to account for unmeasured regions at high values of p_T. Exponential dependence on transverse mass m_T is assumed:

$$\frac{1}{p_T}\frac{d^2n}{dp_T\,dy} = \frac{dn/dy}{T\cdot(m_K+T)}\cdot e^{-(m_T-m_K)/T} \tag{4.1}$$

The function is fitted in the acceptance region and its integral beyond the acceptance is added to the measured data. The contribution of the extrapolation is typically of the order of 1%.

The fit of transverse momentum spectra with Eq. 4.1 determines the inverse slope parameter T. The results obtained for Be+Be interactions are shown and compared to other systems in Fig. 5.
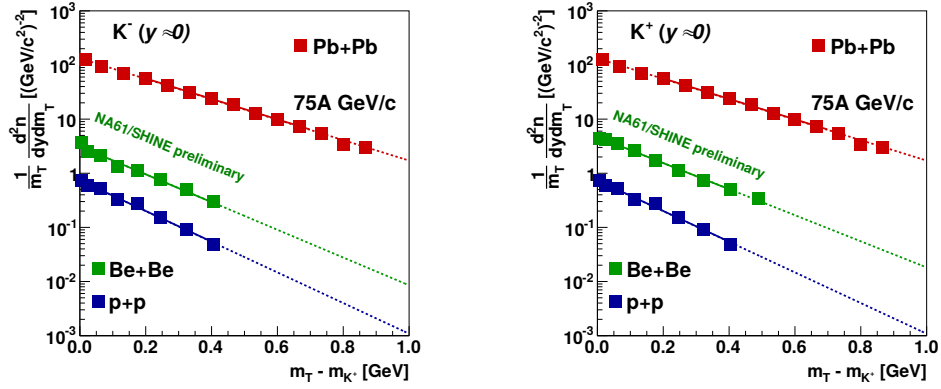
Figure 4: Transverse mass spectra of kaons (K^-, K^+) produced in the 20% most central Be+Be collisions at 150A GeV/c – preliminary results compared to earlier data on p+p interactions from NA61 [4] and central Pb+Pb collisions from NA49 [8].
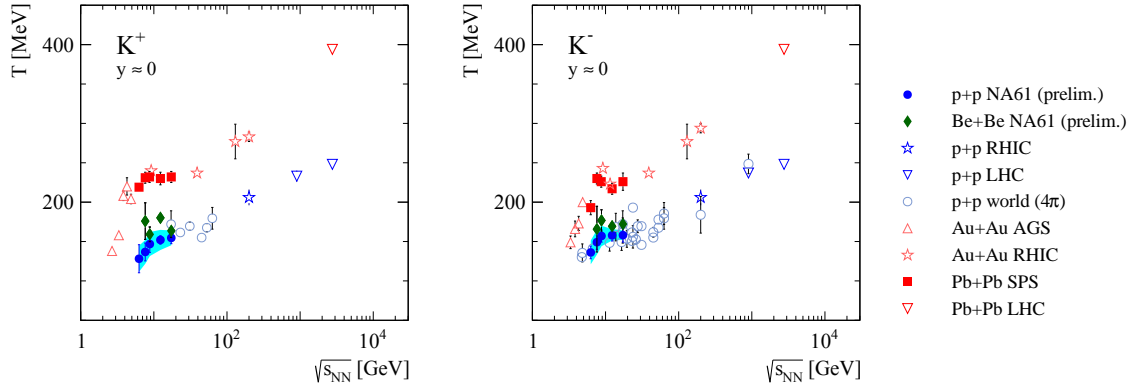

Figure 5: Inverse slope parameter T of charged kaons' (K^+, K^-) transverse mass spectra at mid-rapidity. Preliminary measurements of kaons produced in Be+Be collisions (green diamonds) show values close to the ones obtained for p+p interactions (blue circles). T measured in Pb+Pb interactions (red squares) is significantly higher.

5. Rapidity Spectra

The double differential spectra $\frac{d^2n}{dy\,dp_T}$ described in the previous section are integrated with respect to transverse momentum p_T to calculate the distribution $\frac{dn}{dy}$ of rapidity. The data points are obtained in the acceptance region of the relevant particle identification methods and are shown in Fig. 6. In order to obtain the 4π full phase space mean kaon multiplicity, the $\frac{dn}{dy}$ spectra are extrapolated into the high rapidity region and (if needed, as in the Ar+Sc analysis) interpolated in the mid-rapidity region.

Measured points of the rapidity distributions are reflected with respect to y=0 and a fit is performed with two symmetrically displaced Gaussian functions (see Fig. 7):

$$f_{fit}(y) = \frac{A}{\sigma\sqrt{2\pi}} \exp\left(-\frac{(y-y_0)^2}{2\sigma^2}\right) + \frac{A}{\sigma\sqrt{2\pi}} \exp\left(-\frac{(y+y_0)^2}{2\sigma^2}\right) \tag{5.1}$$
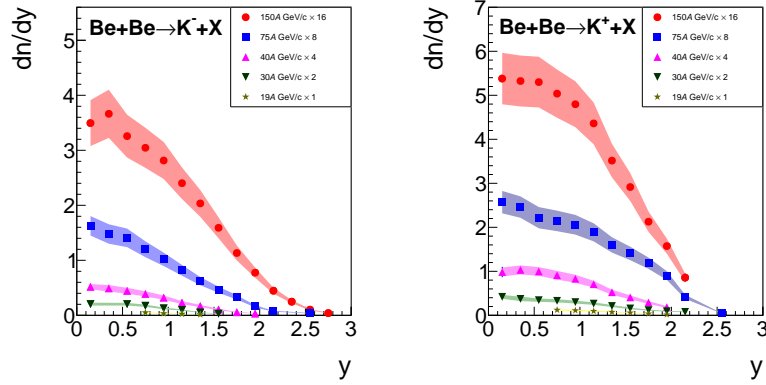

Figure 6: Spectra of rapidity *y* for charged kaons (K^+, K^-) produced in the 20% most central Be+Be collisions at five beam momenta – preliminary results. Note that results for different energies are scaled for better visibility.
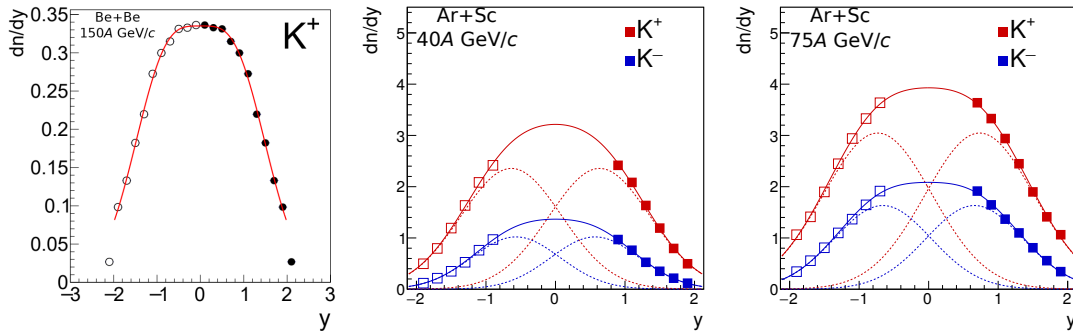

Figure 7: Preliminary results on spectra of rapidity *y* for charged kaons (K^+, K^-) produced in the 20% most central Be+Be interactions at 150*A* GeV/*c* interactions (left) and 5% most central Ar+Sc collisions at 40*A* GeV/*c* (center) and 75*A* GeV/*c* (right). In order to extract mean multiplicities in 4π acceptance the measured points are reflected w. r. t. $y = 0$ and fitted with two symmetrically displaced Gaussians.

6. Proton rapidity spectra

The measurement of the proton rapidity spectrum in Be+Be collisions allows to observe yet another similarity to p+p interactions. As seen in Fig. 8 the shape of proton spectra is similar for Be+Be and p+p at all measured collision energies. The proton spectra measured in Pb+Pb interactions however change significantly with collision energy and the distribution is qualitatively different at lower beam momenta.
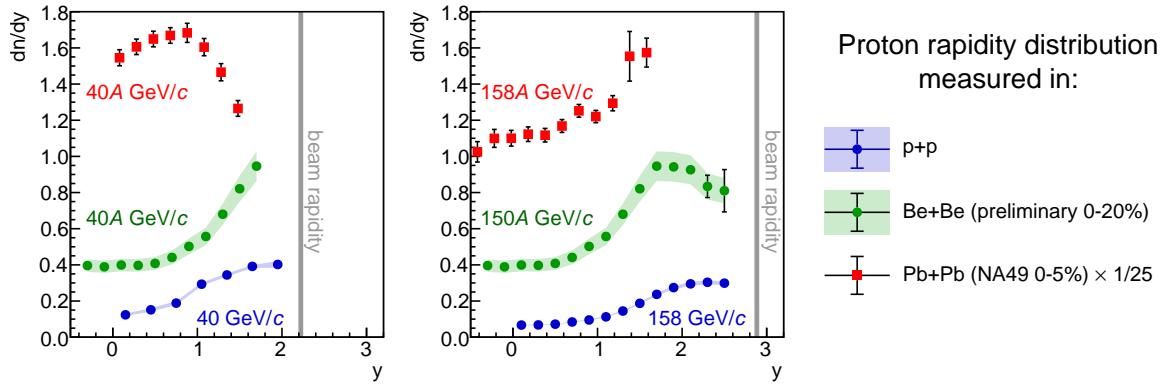
Figure 8: Comparison of proton rapidity spectra measured in p+p, Be+Be (preliminary) and Pb+Pb interactions. One can see a pronounced qualitative difference of the spectrum between light systems (p+p, Be+Be) and Pb+Pb at 40A GeV/c.

7. Mean Kaon Multiplicities

In order to obtain the mean kaon multiplicities $\langle K^+ \rangle$ and $\langle K^- \rangle$, the rapidity spectra $\frac{dn}{dy}$ are integrated by taking the sum of measurements in the acceptance region (forward rapidity) and the integral of the fitted function outside the acceptance (mid-rapidity and $y > 2.0$). Such a calculation is clearly prone to significant uncertainty – for a more detailed discussion please see Ref. [9]. Obtained results for the K/π ratios along with uncertainty estimates for Be+Be and Ar+Sc collisions can be viewed in Figs. 9,10.

7.1 System size dependence of kaon production

Particle production changes rapidly with collision energy in the vicinity of the onset of deconfinement. One observes a clear, qualitative difference between results obtained in p+p collisions and central collisions of heavy nuclei (Pb+Pb or Au+Au). This difference is especially pronounced in the production of strange hadrons (results from heavy-ions exhibit a so-called *horn*) as exemplified by the plots shown in Fig. 10. It is not clear what kind of behavior we should expect for intermediate mass systems (Be+Be, Ar+Sc).

The ratios of mean multiplicites $\langle K^+ \rangle / \langle \pi^+ \rangle$ and $\langle K^- \rangle / \langle \pi^- \rangle$ measured in central Be+Be and Ar+Sc collisions at beam momenta of 30A and 75A GeV/c are compared in Fig. 9 with results from other systems:

- p+p interactions (30, 80 GeV/c) [4]
- central Pb+Pb collisions (30A, 80A GeV/c) [8, 10]

In the calculation of the $\langle K^+ \rangle / \langle \pi^+ \rangle$ ratio for Ar+Sc collisions an approximation had to be made. In the absence of a measurement of $\langle \pi^+ \rangle$ the mean negative pion multiplicity $\langle \pi^- \rangle$ [11] was used instead assuming isospin symmetry: $\langle \pi^+ \rangle \approx \langle \pi^0 \rangle \approx \langle \pi^- \rangle$.

The analysis of particle ratios: $\langle K^+ \rangle / \langle \pi^+ \rangle$, $\langle K^- \rangle / \langle \pi^- \rangle$ reveals a general trend in particle production properties: measurements obtained for central Be+Be collisions fall close to p+p or even below them, while results on most central Ar+Sc interactions lie in between the data on p+p and central Pb+Pb collisions. In particular (see Fig. 9):

- The $\langle K^+ \rangle / \langle \pi^+ \rangle$ ratio at lower beam momenta is similar for p+p and Be+Be and Ar+Sc is only a little higher. At higher collision energies results for Ar+Sc approach those of Pb+Pb while for Be+Be they increases with respect to p+p for the 4π measurement, but stay similar to p+p for the mid-rapidity measurement.
- The $\langle K^- \rangle / \langle \pi^- \rangle$ ratio at mid-rapidity is lower for Be+Be than for p+p. However, this is not the case in 4π acceptance, where they are similar. The ratio obtained for Ar+Sc is once again found in between p+p and Pb+Pb results and approaches the latter at higher collision energies.
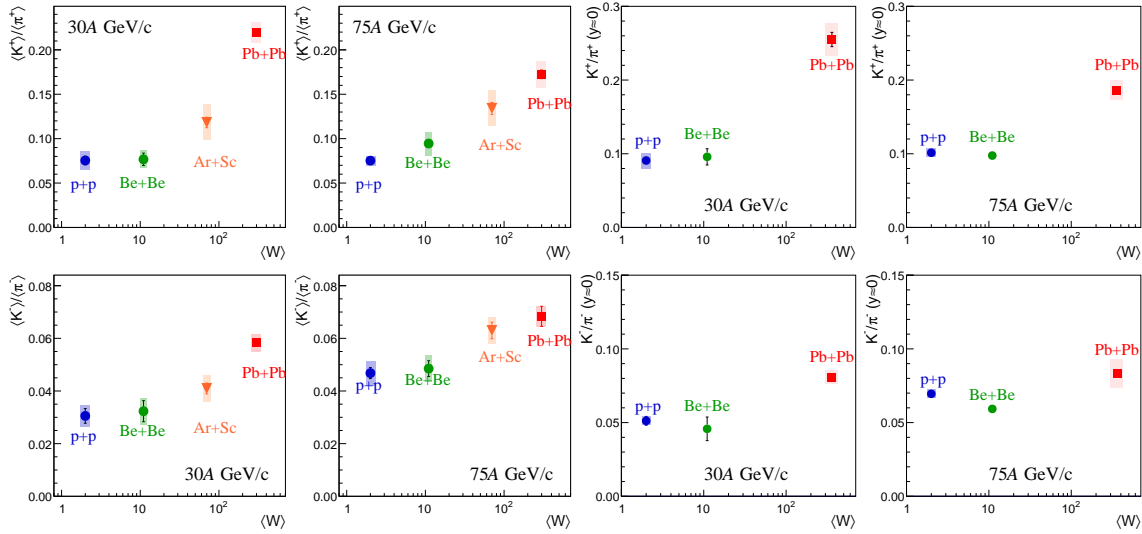

Figure 9: System size dependence of $\langle K^+ \rangle / \langle \pi^+ \rangle$ and $\langle K^- \rangle / \langle \pi^- \rangle$ ratios. Preliminary results on central Ar+Sc interactions lie between earlier measurements in p+p and central Pb+Pb collisions for all studied momenta whereas Be+Be results stay close to p+p measurements. Left plots show 4π acceptance and plots on the right show mid-rapidity results.

7.2 Collision energy dependence of kaon production

The ratio of $\langle K^+ \rangle / \langle \pi^+ \rangle$ was also studied as function of the energy of the colliding nuclei. Figure 10 shows the new results on Be+Be (in 4π acceptance and at mid-rapidity) and central Ar+Sc (in 4π) collisions compared to the available World data. On both plots we can see a clear peak at about 7 GeV (the *horn*) in the results on central heavy-ion collisions as well as its absence in case of p+p interactions. NA61's new results on Be+Be collisions are near results from p+p reactions and do not show any similarity to the horn structure present in heavy-ion data. No "horn" structure is observed in Ar+Sc results either, but the value of the ratio is significantly higher than measured for p+p collisions.

8. Summary

Preliminary results from the CERN SPS on charged kaon production in the 5% most central Ar+Sc and 20% most central Be+Be collisions at beam momenta in the range $19A - 150A$ GeV/c were presented.
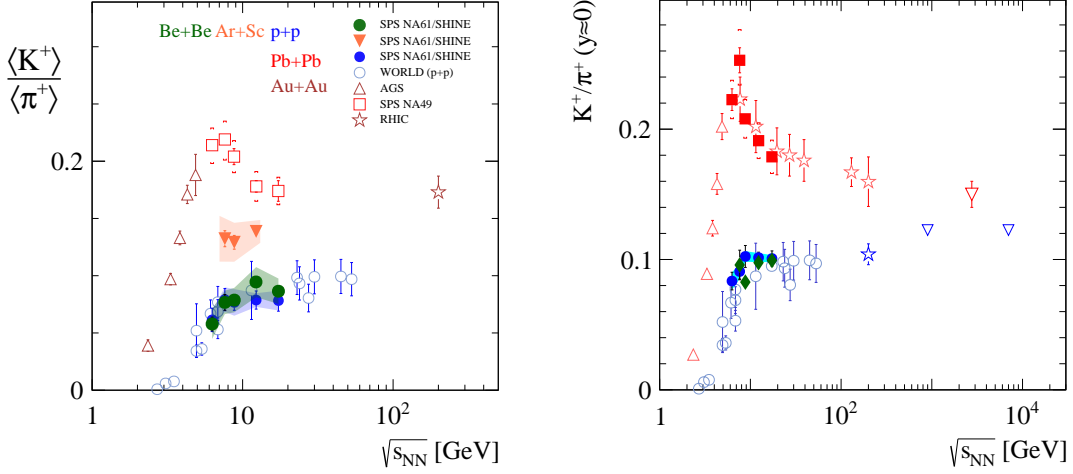
Figure 10: Collision energy dependence of the $\langle K^+ \rangle / \langle \pi^+ \rangle$ ratio for 4π acceptance and K^+/π^+ yields at mid-rapidity. Newly obtained results for Be+Be are close to the values obtained for p+p and recent results for Ar+Sc collisions lie between data for heavy (Pb+Pb) and light systems (Be+Be, p+p). No "horn" structure is visible in either the Be+Be or the Ar+Sc system.

The recent measurements of Be+Be interactions include spectra of transverse momentum and rapidity of $\pi^\pm, K^\pm$ and p. The results concerning kaons (K^+ and K^-) were reviewed in detail and yields at mid-rapidity and full phase-space (4π) were calculated.

The inverse slope parameter T, extracted from mid-rapidity transverse mass spectra of kaons (K^+, K^-), measured for Be+Be collisions is close to results from p+p interactions. As was already shown in Ref. [9] kaon transverse momentum spectra in central Ar+Sc reactions more closely resemble central Pb+Pb collision data.

Interesting behavior is seen in the rapidity distribution of protons produced in Be+Be collisions. At $40A$ GeV/c spectra measured for p+p and Be+Be interactions are similar (shape-wise) and qualitatively different from those in central Pb+Pb collisions. However at $150A$-$158A$ GeV/c the shapes of proton rapidity spectra of all three systems are similar. These results can be used as an input to studies of the stiffness of the equation of state in ultrarelativistic collisions.

The measurements of the $\langle K^+ \rangle / \langle \pi^+ \rangle$ and $\langle K^- \rangle / \langle \pi^- \rangle$ ratios show similar trends in their system size dependence, i.e. data on Be+Be is usually closer to p+p, while results on Ar+Sc are in between those from p+p and Pb+Pb. However, results of mid-rapidity measurements of $\langle K^- \rangle / \langle \pi^- \rangle$ for Be+Be are lower than for p+p interactions.

In case of the Ar+Sc system the collision energy dependence is moderate in the measured range for all studied particle ratios. The ratio of $\langle K^+ \rangle / \langle \pi^+ \rangle$ in both Be+Be and Ar+Sc systems, shows no indications of a horn structure in the studied energy range.

Both system size and collision energy dependence of measured observables are not well understood at present and theoretical models (e. g.: SMES [2], PHSD [12]) are unable to reproduce them comprehensively. In the near future we can expect more results from the NA61/SHINE system size scan: completion of analyses of Be+Be and Ar+Sc interactions, as well as brand new results on Xe+La collisions.

References

[1] N. Abgrall *et al.* [NA61/SHINE Collaboration], JINST 9 (2014) P06005.

[2] M. Gazdzicki, M. I. Gorenstein, Acta Phys. Polon. B 30 (1999) 2705.

[3] M.Gazdzicki, P.Seyboth, Acta Phys. Polon. B47 (2016) 1201

[4] A. Aduszkiewicz *et al.* [NA61/SHINE Collaboration], Eur. Phys. J. C 77 (2017) 671.

[5] M. Gazdzicki *et al.*, Phys. Rev. C 83 (2006) 054907.

[6] K. Werner, F. Liu and T. Pierog, Phys. Rev. C 74 (2006) 044902.

[7] N. et al. Abgrall *et al.* [NA61/SHINE Collaboration], Eur. Phys. J. C 74 (2014) 1.

[8] C. Alt *et al.* [NA49 Collaboration], Phys. Rev. C 77 (2008) 024903.

[9] M. P. Lewicki [NA61/SHINE Collaboration], PoS CPOD2017 (2018) 057.

[10] S. V. Afanasiev *et al.* [NA49 Collaboration], Phys. Rev. C 66 (2002) 054902.

[11] M. Naskręt, Acta Phys. Polon. Supp. **10**, 693 (2017)

[12] A. Palmese, et al. Phys. Rev. C 94, no. 4, 044912 (2016)

PoS(CORFU2018)166